scientific reports

Check for updates

OPEN

# Generation of "OP7 chimera" defective interfering influenza A particle preparations free of infectious virus that show antiviral efficacy in mice

Tanya Dogra[1], Lars Pelz[1], Julia D. Boehme[2,3], Jan Kuechler[1], Olivia Kershaw[4], Pavel Marichal-Gallardo[1], Maike Baelkner[2,3], Marc D. Hein[5], Achim D. Gruber[4], Dirk Benndorf[1,5], Yvonne Genzel[1], Dunja Bruder[2,3], Sascha Y. Kupke[1]✉ & Udo Reichl[1,5]

**Influenza A virus (IAV) defective interfering particles (DIPs) are considered as new promising antiviral agents. Conventional DIPs (cDIPs) contain a deletion in the genome and can only replicate upon co-infection with infectious standard virus (STV), during which they suppress STV replication. We previously discovered a new type of IAV DIP "OP7" that entails genomic point mutations and displays higher antiviral efficacy than cDIPs. To avoid safety concerns for the medical use of OP7 preparations, we developed a production system that does not depend on infectious IAV. We reconstituted a mixture of DIPs consisting of cDIPs and OP7 chimera DIPs, in which both harbor a deletion in their genome. To complement the defect, the deleted viral protein is expressed by the suspension cell line used for production in shake flasks. Here, DIP preparations harvested are not contaminated with infectious virions, and the fraction of OP7 chimera DIPs depended on the multiplicity of infection. Intranasal administration of OP7 chimera DIP material was well tolerated in mice. A rescue from an otherwise lethal IAV infection and no signs of disease upon OP7 chimera DIP co-infection demonstrated the remarkable antiviral efficacy. The clinical development of this new class of broad-spectrum antiviral may contribute to pandemic preparedness.**

Influenza A virus (IAV) is a major human pathogen. Infections cause annual epidemics, which lead to excessive morbidity and mortality[1]. When novel strains emerge, IAV infections may result in a severe pandemic, which is considered an imminent threat. For instance, more than 40 million deaths were reported during the "Spanish flu" in 1918[2]. Annual prophylactic vaccination is the most effective measure to prevent seasonal influenza infection[3]. Yet, the selection of strains as well as the manufacturing and release of seasonal vaccines requires several months. Thus, small-molecule drug antivirals are also used, for instance, to treat acute infections[1]. However, circulating human IAV strains have acquired resistance against many current antivirals[3]. Therefore, new broadly-acting antiviral treatment options should be considered not only to complement annual vaccination schemes but also to act as a first line of defense for pandemic preparedness.

Defective interfering particles (DIPs) are regarded as a promising new class of antivirals[4–17]. In particular, DIPs resulted in a high tolerability and antiviral efficacy in animal studies[5,16,18–25], and were therefore proposed as prophylactic and therapeutic antivirals[16,25–27]. IAV DIPs typically contain a large internal deletion in one of the eight genomic viral RNA (vRNA) segments[4,10,16,22,25,26,28–30]. The missing genomic information results in the expression of a truncated viral protein[31]. Therefore, DIPs are defective in virus replication and cannot propagate in mammalian cells. In a co-infection with an infectious standard virus (STV), however, the missing gene

[1]Max Planck Institute for Dynamics of Complex Technical Systems, Bioprocess Engineering, Magdeburg, Germany. [2]Institute of Medical Microbiology, Infection Prevention and Control, Infection Immunology Group, Health Campus Immunology, Infectiology and Inflammation, Otto Von Guericke University Magdeburg, Magdeburg, Germany. [3]Immune Regulation Group, Helmholtz Centre for Infection Research, Braunschweig, Germany. [4]Department of Veterinary Pathology, Freie Universität Berlin, Berlin, Germany. [5]Bioprocess Engineering, Otto Von Guericke University Magdeburg, Magdeburg, Germany. ✉email: kupke@mpi-magdeburg.mpg.de

function (i.e., the full-length (FL) protein) is provided, and DIPs can propagate. Interestingly, this results in a strong interference with STV replication. With respect to this antiviral effect, it is suggested that the short defective interfering (DI) vRNAs replicate faster and accumulate to higher levels than the FL vRNAs. Thereby, cellular and viral resources are depleted, which suppresses infectious virus replication[32–34]. DIP co-infections also result in a strong induction of the interferon (IFN) system[35–38], and it was shown that this stimulation of the innate immunity also contributes to their antiviral effect[25,26,35,37]. As a consequence, IAV DIPs display a broad-spectrum antiviral activity that is not only directed against a wide range of IAV strains[16,21,25,39,40], but even against unrelated viruses, including SARS-CoV-2[37,38,41,42].

Previously, we developed a cell culture-based production process[18,43] for a well-known DIP called "DI244" that harbors a deletion in segment 1 (Seg 1)[25,26]. DI244 is unable to express the viral polymerase basic protein 2 (PB2, encoded from Seg 1) and can be propagated in genetically engineered PB2-expressing Madin-Darby canine kidney (MDCK) suspension (MDCK-PB2(sus)) cells[18,43,44]. In addition, using a modified reverse genetics workflow for IAV that is specific for DIP rescue, clonal DI244 without STVs could be reconstituted for production[44]. Therefore, considering the use of DIPs as an antiviral, the absence of infectious STVs is expected to alleviate potential safety and regulatory concerns.

We previously discovered a new type of IAV DIP, called "OP7" that contains multiple point substitutions on segment 7 (Seg 7) vRNA instead of a large internal deletion[39]. OP7 showed a higher antiviral activity compared to Seg 1 conventional DIPs (cDIPs) including DI244 as shown in in vitro and in vivo experiments[18,19,37]. As the source of the defect in virus replication of OP7 is yet unknown, designing a cell line that could complement the defect of OP7 was not feasible, so far. Instead, we recently established a cell culture-based production process for OP7 in the presence of infectious STVs to complement the unknown defect[19]. However, infectious STVs had to be UV-inactivated, which also reduced the antiviral activity of OP7. Moreover, even after UV treatment, the risk of contamination with residual STVs should raise safety concerns concerning medical application.

In the present study, we devised a genetically engineered cell culture-based production system for OP7, which does not require the addition of any infectious STV. Trials in mice suggest that the produced OP7 preparations can be used as a safe and potent antiviral, and further steps towards clinical development seem promising.

## Results

### Reconstitution of OP7 chimera DIPs without infectious STVs

Previously, OP7 was produced in cell culture in the presence of infectious STVs[19]. To obtain an OP7 virus without infectious STVs (STV-free), we modified a plasmid-based reverse genetics system for the reconstitution of Seg 1-derived cDIPs based on the IAV strain A/PR/8/34 (PR8) as described previously[44]. As Seg 1 cDIPs contain a large internal deletion in Seg 1 and are unable to express the viral PB2 protein, the STV-free reconstitution of clonal Seg 1 cDIPs requires PB2-expressing cells (Fig. 1A–C). Here, a co-culture of adherent PB2-expressing human embryonic kidney (HEK-293T-PB2(adh)) and MDCK-PB2(adh) cells (Fig. 1B) were co-transfected with eight plasmids encoding for the deleted Seg 1 and the remaining seven wild-type (WT) segments (Fig. 1A). After reconstitution, such Seg 1 cDIPs (Fig. 1C) could be propagated in cell culture using PB2-expressing cells, as shown previously[18,43,45].

To reconstitute OP7 chimera DIPs without infectious STVs, we added a ninth plasmid encoding for the mutated Seg 7 of OP7 (Seg 7-OP7) (Fig. 1D) for transfection. This resulted in the rescue of a population of two types of DIPs: (i) Seg 1 cDIPs (Fig. 1C) and (ii) OP7 chimera DIPs (Fig. 1E). Accordingly, the Seg 1 cDIPs contained a truncated Seg 1 vRNA and seven WT vRNAs (Fig. 1C) and OP7 chimera DIPs contained Seg 7-OP7 vRNA, a truncated Seg 1 vRNA, and the remaining six WT vRNAs (Fig. 1E). Owing to a deletion in Seg 1 (encoding for PB2), both DIPs could be propagated in MDCK-PB2(sus) cells (Fig. 2). Furthermore, it has to be assumed that the OP7 chimera DIPs (Fig. 1E) are defective in virus replication in PB2-expressing cells, as they contain the mutated and defective Seg 7-OP7 vRNA. Accordingly, for propagation, OP7 chimera DIPs require complementation with Seg 1 cDIPs (Fig. 1C) as they provide the functional Seg 7-WT vRNA (Seg 7-WT). Moreover, as both DIPs (Fig. 1C,E) are replication deficient in non-PB2 expressing cells, we eliminate the need for post-production UV inactivation due to the lack of infectious STVs. Note that the deleted Seg 1 sequence used in the present study was previously identified by us ("Seg 1 gain"), where corresponding DIPs showed a superior in vitro interfering efficacy compared to the well-known DI244[45]. A seed virus stock was generated from the reconstituted OP7 chimera DIP material by serial passaging in MDCK-PB2(adh) followed by MDCK-PB2(sus) cells. This seed virus was used for subsequent cell culture-based production (Fig. 2). The absence of infectious STVs in the produced OP7 chimera DIP material was evaluated by two serial passages in adherent WT MDCK (MDCK(adh)) cells (innocuity assay). Both passages showed no virus titer, thus confirming no infectious STV replication (data not shown).

In summary, we reconstituted OP7 chimera DIPs in a mixture with Seg 1 cDIPs without the addition of any infectious STVs. Seg 1 cDIPs can complement the defect of the OP7 chimera DIPs in PB2-expressing MDCK cells, allowing for cell culture-based production.

### Cell culture-based production of OP7 chimera DIP preparation in shake flasks shows a strong dependence on the multiplicity of infection

As indicated above, OP7 chimera DIPs are defective in virus replication in MDCK-PB2(sus) cells and propagation requires co-infection with Seg 1 cDIPs. Previously, in a similar production system, we produced OP7 in the presence of infectious STVs in WT MDCK(sus) cells. As expected for virus production, total virus yields were multiplicity of infection (MOI) dependent[19]. High MOI conditions increased the likelihood of co-infection of STVs and OP7, resulting in preferential production of OP7 that suppressed STV propagation and thus, total virus yields. In contrast, in a low MOI scenario, more single hit infections occurred. Therefore, STV growth

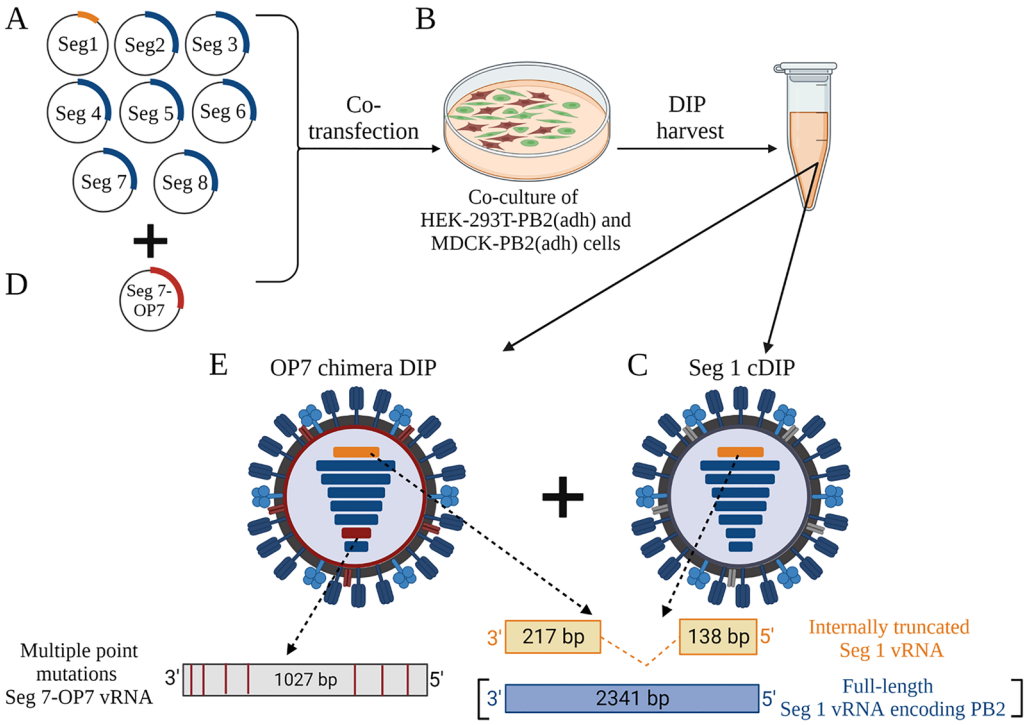


**Figure 1.** Plasmid-based reconstitution of OP7 chimera DIPs free of infectious STVs. Rescue of Seg 1 conventional DIPs (cDIPs). The reverse genetics system comprises (**A**) eight plasmids that encode for a deleted Seg 1 vRNA and Seg 2–8 wild type (WT) vRNAs. (**B**) Co-transfection of a co-culture of PB2-expressing HEK-293T-PB2(adh) (high transfection efficiency) and MDCK-PB2(adh) (high virus titers) cells results in reconstitution of (**C**) clonal Seg 1 cDIP free of infectious standard viruses (STV). Rescue of OP7 chimera DIPs: addition of a (**D**) ninth plasmid that encodes for the mutated Seg 7-OP7 vRNA results in the reconstitution of a mixture of DIPs including (**E**) OP7 chimera DIPs and (**C**) Seg 1 cDIPs. This mixture of viruses can be propagated in MDCK-PB2(sus) cells (Fig. 2). Image was created with BioRender.com.

occurred predominantly and the propagation-incompetent OP7 was out-diluted, resulting in higher total virus titers with a concomitant lower fraction of OP7[19]. We expected that the DIP mixture containing OP7 chimera DIPs and Seg 1 cDIPs would show the same MOI dependency in PB2-expressing cells. Thus, to optimize total virus yields and the fraction of OP7 chimera DIPs within the mixture, we performed infections in shake flasks using MDCK-PB2(sus) cells at different MOIs ranging from 1E-2 to 1E-5 (Fig. 2).

After infection at $2.1 \times 10^6$ cells/mL, cells continued to grow (Fig. 2A). The viable cell concentration (VCC) post infection at an MOI of 1E-2 peaked fastest ($3.0 \times 10^6$ cells/mL, 18 hpi) before there was a decrease in VCC. With decreasing MOIs, the maximum VCC increased and cell death started later. As expected, the hemagglutinin (HA) titer (indicating total virus yield) reached lower values at higher MOIs relative to lower MOIs (Fig. 2B), likely due to the inhibition caused by the increasing accumulation of OP7 chimera DIPs towards higher MOIs. This is in line with greater fractions of OP7 chimera DIPs at higher MOIs (Fig. 2C,D). For instance, we found a fraction of OP7 chimera DIPs of 94.4% (MOI 1E-2) and 24.2% (MOI 1E-5), calculated based on the extracellular vRNA concentration of Seg 7-OP7 and Seg 7 of the WT virus quantified by reverse transcription real time PCR (RT-qPCR) (Fig. 2C). In addition, quantification of IAV proteins by a new mass spectrometry (MS) method developed in our group[46] showed similar fractions of 90.2% (MOI 1E-2) and 19.0% (MOI 1E-5). Here the fraction was calculated based on the concentration of the extracellular matrix protein 1 (M1, encoded on Seg 7) of OP7 (M1-OP7) and of the WT virus (M1-WT) (Fig. 2D). Further, the total virus concentration (as indicated by the extracellular Seg 5 vRNA concentration (Fig. 2C) and calculated from the nucleoprotein (NP) concentration (Fig. 2D)) showed higher values for lower MOIs in line with HA titers (Fig. 2B). Previously, biological activity of IAV particles decreased over time as seen by a drop in the infectious virus titers towards late process times[47], which is important for selecting the optimal harvest time point (Fig. 2B). Accordingly, for DIP harvesting, we selected the time point at which the HA titer almost plateaued to ensure maximum virus release and biological activity of the DIPs (MOI 1E-2: 25 hpi, MOI 1E-3: 32 hpi, MOI 1E-4: 40 hpi, MOI 1E-5: 48 hpi). Furthermore, harvesting was performed no later than the onset of cell death (Fig. 2A) to avoid excessive levels of cell debris and host cell DNA in the supernatant that would otherwise interfere with the subsequent downstream purification process. Further, final viral harvests were DIP depleted as we did not observe a strong accumulation of other DI vRNAs in Seg 2–8 as suggested by results from RT-PCR (Fig. 3).

Taken together, our results demonstrate that the MOI has a strong effect on OP7 chimera DIPs production. At high MOI, high fractions of OP7 chimera DIPs were present along with low total virus titers suggesting that OP7 chimera DIPs impeded virus propagation. On the other hand, higher total virus titers, but lower fractions

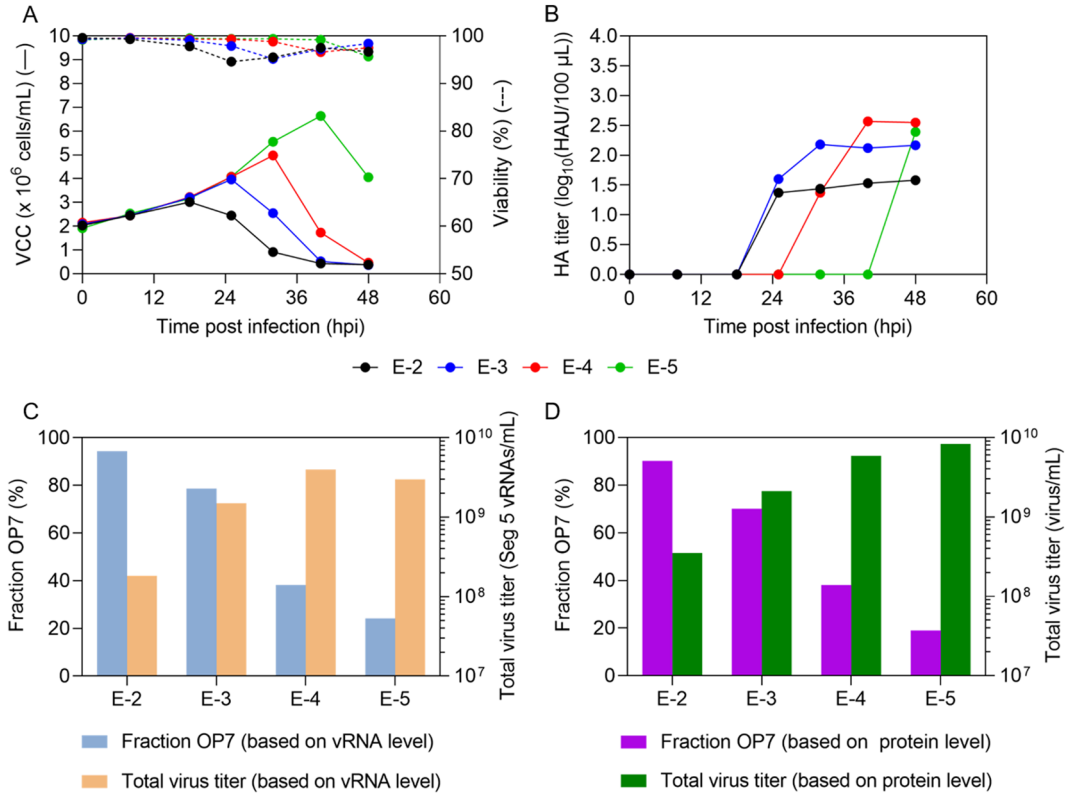


**Figure 2.** Cell culture-based production of OP7 chimera DIP enriched material in shake flasks. Genetically engineered MDCK-PB2(sus) cells cultivated in 125 mL shake flasks (50 mL working volume), were infected at multiplicity of infections (MOIs) ranging from 1E-2 to 1E-5 after a complete medium exchange. (**A**) Viable cell concentration (VCC) and viability. (**B**) Hemagglutinin assay (HA) titer. (**C**) Fraction of OP7 chimera DIPs (calculated based on extracellular Seg 7-OP7 and Seg 7-WT vRNA concentrations, quantified by reverse transcription real time PCR (RT-qPCR). Total virus concentration is indicated by the extracellular Seg 5 vRNA concentration. (**D**) Fraction of OP7 chimera DIPs (calculated based on extracellular M1-OP7 and M1-WT viral protein concentrations, quantified by Mass spectrometry (MS). Total virus concentration was calculated from the protein concentration of nucleoprotein (NP), encoded by Seg 5. The optimal harvest time points (MOI 1E-2: 25 hpi, 1E-3: 32 hpi, 1E-4: 40 hpi, 1E-5: 48 hpi) were analyzed for C and D. The figure depicts the results of one experiment.

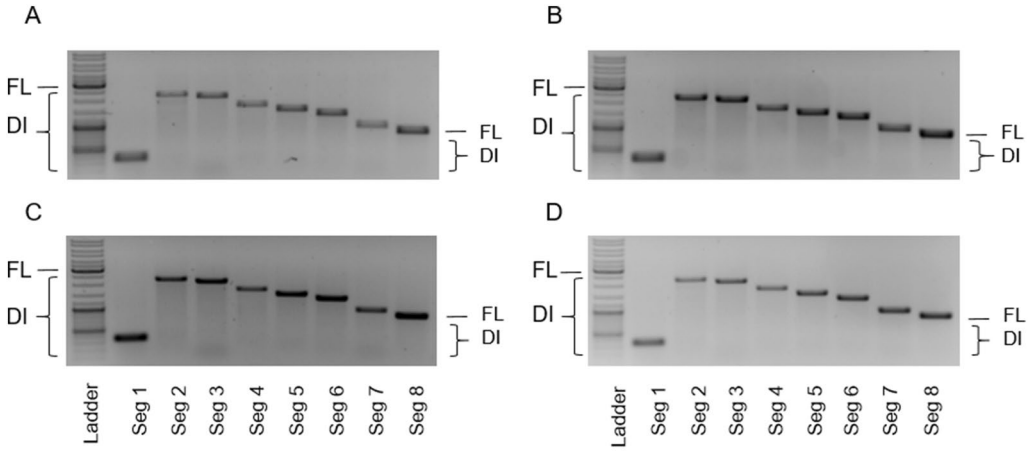


**Figure 3.** Purity of produced OP7 chimera DIP material with respect to contaminating DIPs. OP7 chimera enriched DIPs were produced at different MOIs in shake flasks (Fig. 2). Samples from 48 hpi were subjected to segment-specific reverse transcription PCR (RT-PCR) and gel electrophoresis. (**A**) MOI 1E-2, (**B**) MOI 1E-3, (**C**) MOI 1E-4, and (**D**) MOI 1E-5. The indicated signals correspond to FL and DI vRNAs. Upper thicker band of the ladder: 3000 bp, middle thicker band: 1000 bp, lower thicker band: 500 bp. Cropped gels are shown; original gels are presented in Supplementary Fig. S1.

of OP7 chimera DIPs were found at lower MOIs. Infections at intermediate MOIs of 1E-3 and 1E-4 appear to be a good compromise for achieving high OP7 chimera DIP fractions and high virus titers.

## The MOI used for production affects the in vitro interfering efficacy

To identify the optimal MOI yielding OP7 chimera DIP material showing the highest in vitro interfering efficacy per product volume an in vitro interference assay (Fig. 4) was carried out. In brief, WT MDCK(adh) cells were either infected with STVs only at a MOI of 10 (negative control, NC) or co-infected with 125 µL (fixed volume) of DIP material produced at different MOIs (Fig. 2).

Our results indicated the strongest interfering efficacy for the OP7 chimera DIP material produced at a MOI of 1E-3 and 1E-4. This was shown by a suppression of the infectious virus release by more than two orders of magnitude (quantified by the plaque assay), which was significantly more than the decrease of only a factor of two, observed for the material produced at a MOI of 1E-2 ($p < 0.0001$, One-way analysis of variance (ANOVA) followed by Tukey´s multiple comparison test), and significantly different to the reduction of one log for the material produced at a MOI of 1E-5 ($p < 0.001$) (Fig. 4A). For the total virus release, as expressed by the HA titer (Fig. 4A) and extracellular Seg 5 vRNA concentration (Fig. 4B), this trend was less pronounced. Further, co-infections with highly interfering DIP material, produced at a MOI of 1E-3 and 1E-4, resulted in a pronounced OP7 phenotype, i.e. an overproportional extracellular Seg 7-OP7 vRNA concentration in comparison to other gene segments[19,39], indicating the preferential replication of Seg 7-OP7 vRNA during virus propagation (Fig. 4B). Similarly, an overproportional M1-OP7 concentration relative to M1-WT was found in progeny virions (Fig. 4C).

In summary, the interfering efficacy of OP7 chimera DIP preparations strongly depended on the MOI for production with intermediate MOIs of 1E-3 and 1E-4 representing the optimum.

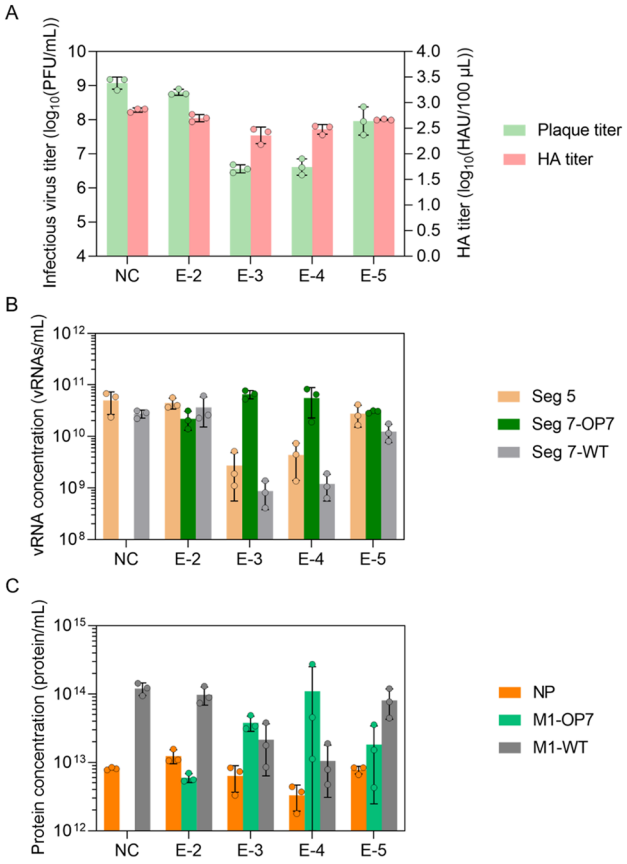


**Figure 4.** In vitro interference assay with OP7 chimera DIP enriched material produced at different MOIs. MDCK(adh) cells were infected with STVs alone at a MOI of 10 (NC) or co-infected with 125 µL of indicated DIP material produced at different MOIs in shake flasks (Fig. 2). (**A**) Infectious virus release, indicated by plaque titer, and total virus release, indicated by HA titer, at 16 hpi. PFU, plaque-forming units; HAU, HA units. (**B**) Extracellular vRNA concentration, quantified by RT-qPCR. (**C**) Protein concentration, quantified by MS. NP, nucleoprotein. Interference assay was performed in three independent experiments, corresponding samples were quantified in a single measurement. Error bars indicate the standard deviation (SD). Samples of the optimal harvest time points (Fig. 2) were analyzed.

### High in vivo tolerability and antiviral efficacy of OP7 chimera DIP material

To test the tolerability and antiviral efficacy of produced OP7 chimera DIP enriched material in a mouse infection model, DIP material produced in shake flasks and purified by steric exclusion chromatography (SXC)[18,19,48,49] was used. The material was produced at MOI 1E-4 ($8.96 \times 10^9$ virions/mL, calculated based on Seg 5 vRNA concentrations; OP7 chimera DIP fraction of 60.07%, calculated based on Seg 7-OP7 and Seg 7-WT vRNA concentrations). As a negative control, an OP7 chimera DIP preparation that was inactivated with UV light for 24 min was utilized, which typically does not show an interfering efficacy in vitro[18,19].

First, to test for the tolerability of the OP7 chimera DIP preparations, we administered 20 µL of active OP7 chimera DIPs (diluted to 1:2 and 1:20, corresponding to $8.96 \times 10^7$ and $8.96 \times 10^6$ virions per mouse, respectively) intranasally to the animals (Fig. 5A–C). Similar to PBS treatment, OP7 chimera enriched DIP treatment was well-tolerated, as indicated by the absence of weight loss (Fig. 5A) and clinical scores (Fig. 5B). Moreover, serum albumin levels in bronchoalveolar lavage (BAL) samples of PBS and OP7 chimera DIP-treated mice were comparable, indicating that OP7 chimera DIP administration did not compromise lung integrity (Fig. 5C), which is otherwise typically observed in influenza-infected mice[50–52]. This was further confirmed by histopathological examination of the lungs. For mice treated with PBS (Fig. 6A), only minimal interstitial pneumonia located near the hilus and affecting less than 5% of the lung tissue was observed; a finding that can be typically attributed to intranasal application of liquid to the lungs. Mice treated with OP7 chimera DIPs (1:2 and 1:20 dilution) showed a minimal increase in inflammatory infiltration with rare lymphocytes detectable in the interstitium and few macrophages and neutrophils in the alveoli (Fig. 6A,B middle and right column) affecting only small parts of the lung tissue at the hilus, too. Yet, no histopathological changes that appear to be clinically relevant were observed, which is in line with the presentation of the clinical scores (Fig. 5B). Together, these data demonstrate that intranasal administration of OP7 chimera DIPs alone is well-tolerated.

Next, we treated mice with a lethal dose of 1000 focus-forming units (FFU) of IAV STV (strain PR8) together with either active OP7 chimera DIPs (1:2 and 1:20), inactive OP7 chimera DIPs (1:2) or PBS (1:2) in a total volume of 20 µL. As expected, severe body weight loss and 100% IAV-induced mortality was observed in PBS co-treated mice (Fig. 5D,F). Further, similar to PBS co-treatment, mice co-treated with inactive OP7 chimera DIPs showed the same high infection-induced morbidity (Fig. 5D,E) and mortality (Fig. 5F), indicating the absence of protective efficacy by UV inactivated DIPs. In strong contrast, no body weight loss was observed when active OP7 chimera DIPs (1:2 diluted) were co-administered, while a higher dilution (1:20) resulted in a modest loss of body weight (approx. 16%). Importantly, all mice co-applied with active OP7 chimera DIPs (1:2 and 1:20) survived the otherwise lethal STV infection (Fig. 5F). Intriguingly, co-administration of active OP7 chimera DIPs (1:2) together with a lethal STV dose completely prevented the development of clinical signs (Fig. 5E) related for influenza infection compared to PBS treatment only (Fig. 5B). Even co-administration of active OP7 chimera DIPs diluted to 1:20 together with a lethal dose of STV was highly effective in preventing a severe course of influenza disease (Fig. 5E). In line with these findings, histopathological analysis revealed only a low-grade pneumonia characterized by mild perivascular and interstitial lymphocytic infiltration, pneumocyte type II hyperplasia and alveolar histiocytosis of mice co-administered with a lethal dose of STVs and OP7 chimera DIPs at a dilution of 1:2 (Fig. 6B middle column). In comparison, a lethal dose of STV of strain PR8 typically resulted in hyper-inflammatory immune responses in infected lungs[53]. Even the co-application of the low (1:20) dose OP7 chimera DIPs was sufficient to protect the animals from a lethal outcome of pneumonia (Fig. 6B right column). Histopathologically, similar qualitative changes were identified in the animals of this group, but the lesion extent was significantly greater with additional onset of interstitial fibrosis and, in isolated cases, low-grade, florid suppurative inflammation.

Taken together, intranasal application of only the OP7 chimera DIP material is very well-tolerated in mice. Furthermore, the co-administration of OP7 chimera DIPs mediated full protection against an otherwise lethal IAV STV infection. These data demonstrate the safety and remarkable antiviral efficacy of the produced OP7 chimera DIPs in vivo.

## Discussion

Previous studies of our group showed that the MOI used for cell culture-based production of DIPs affects total virus yields[18,19,54,55] and interfering efficacy[18,19]. Likewise, in the present work, we found the highest interfering efficacy for material produced at intermediate MOIs of 1E-3 and 1E-4 (Fig. 2). Here, a balanced trade-off between the fraction of OP7 chimera DIPs and total virus yields in the produced material appears to be decisive for the optimal interfering efficacy observed in vitro.

In this study, we also evaluated the tolerability and efficacy of OP7 chimera DIP preparations harvested from shake flasks using a mouse model. Most laboratory mouse strains lack the *Mx1* gene, which is an important IFN-induced restriction factor against IAV infections in mice and in humans. Therefore, we used a mouse model expressing a functional *Mx1* gene, called D2(B6).A2G-*Mx1*$^{r/r}$[53]. Accordingly, this model better represents the immune response in humans to IAV infections. Intranasal administration of high doses of only OP7 chimera DIP enriched preparations did neither result in disease, nor in clinically relevant histopathological changes in mice lungs, indicating a high tolerability after OP7 chimera DIP treatment (Fig. 5A,B,C and Fig. 6A). These results (and those of other groups[5,16,20–25,40]) clearly suggest that common concerns regarding adverse effects (e.g., cytokine storm, lung damage) due to DIP administration in animals can be abandoned and that DIPs, as defective, non-replicating viral particles might also be suitable for safe clinical applications in humans. Moreover, co-infection with a lethal dose of STV together with OP7 chimera DIPs resulted in 100% survival of the mice (Fig. 5F), and these animals did not even show signs of clinical disease (Fig. 5E). A similarly high antiviral activity (against lethal STV infection) was found for DIPs derived from IAV and from other viral species in different animal models[5,16,18–25,40]. Earlier investigations on the use of DIPs as prophylactic antiviral agents have shown promising

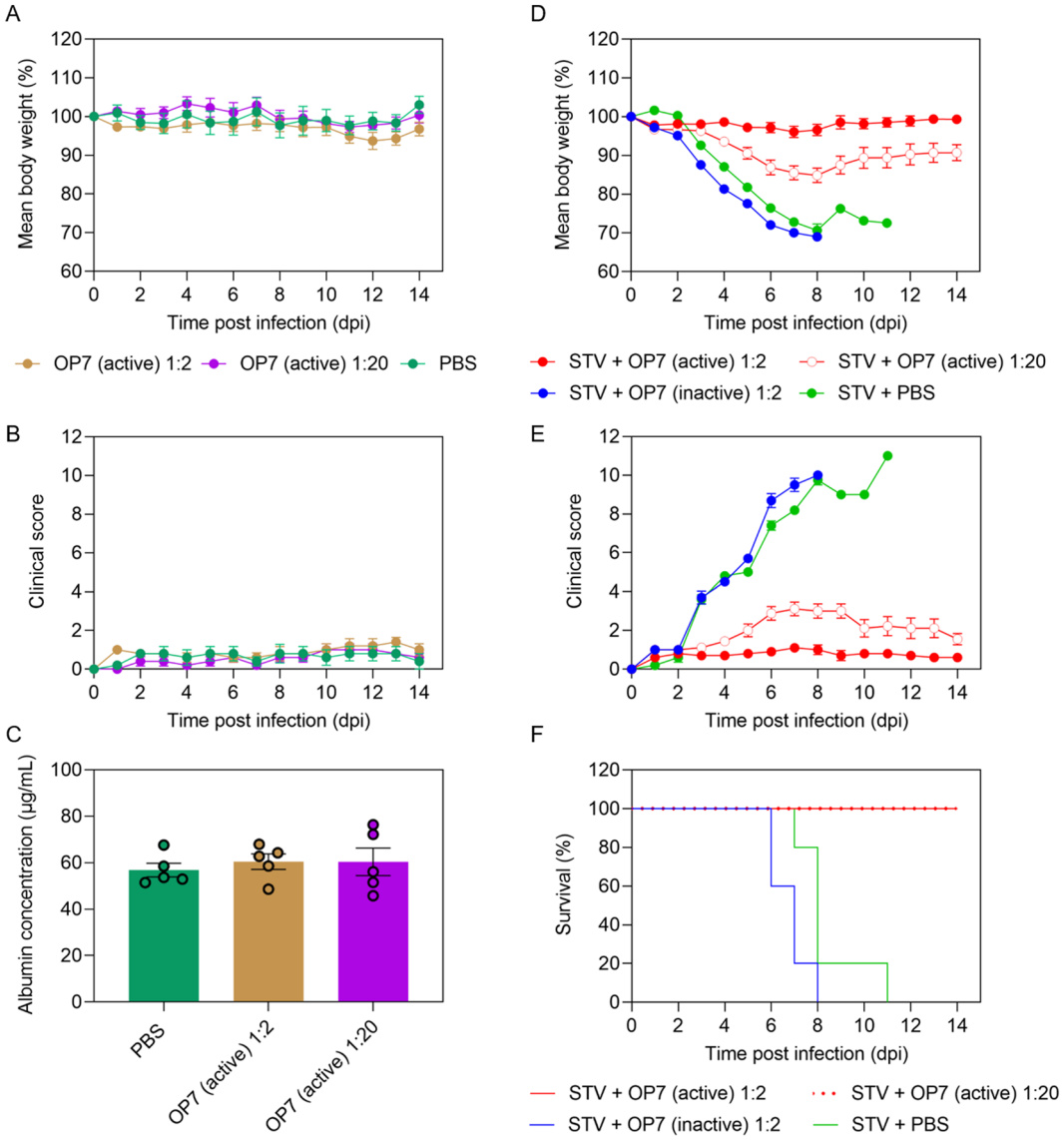


**Figure 5.** In vivo tolerability and antiviral efficacy of OP7 chimera DIP preparations in a mouse infection model. (**A**–**C**) 20 µL of active OP7 chimera DIP material diluted to 1:2 ($8.96 \times 10^7$ virions/mouse) or 1:20 ($8.96 \times 10^6$ virions/mouse), or 20 µL PBS was intranasally administered to 12–24 weeks old female D2(B6).A2G-Mx1$^{r/r}$ mice (n = 5). (**A**) Mean body weight loss. Two-way ANOVA and Tukey correction for multiple comparison did not reveal a significant difference between groups ($p > 0.05$). (**B**) Clinical score. (**C**) Serum albumin concentrations in bronchoalveolar (BAL) fluid were measured by ELISA at 14 dpi. One-way ANOVA did not reveal a significant difference between means ($p > 0.05$). (**D**–**F**) Mice were treated with a lethal dose of 1000 FFU of IAV STV (strain PR8) together with either active OP7 chimera DIPs, diluted to 1:2 (n = 10) or 1:20 (n = 9), inactive OP7 chimera DIPs diluted to 1:2 (n = 10) or PBS (n = 5) in a total volume of 20 µL. (**D**) Mean body weight loss. The differences between the mean body weight of mice co-treated with 1:2 (mixed-effects model and Tukey correction for multiple comparison, $p < 0.0001$) or 1:20 OP7 chimera DIPs ($p < 0.05$) were significant relative to co-treatment with PBS. (**E**) Clinical score. (**F**) Kaplan-Meyer curve representing the survival rate. The differences between the survival of mice co-treated with 1:2 (log-rank test for two groups, $p < 0.0001$) or 1:20 OP7 chimera DIPs ($p < 0.0001$) were significant relative to co-treatment with PBS. (**F**) Clinical score. (**A**–**F**) Error bars indicate the standard error of the mean (SEM).

results[26,27]. Here, mice were intranasally pre-treated with DI244 (a well-characterized Seg 1 cDIP) seven days before infection with a lethal dose of IAV, and the DIP pre-administration continued to provide protection[25]. Also, it was proposed to use DIPs as a therapeutic treatment due to its early onset of antiviral activity. Again, DI244 administered one or two days after lethal IAV challenge rendered full or partial protection, respectively[25].

In light of imminent pandemic threats, new broadly-acting antivirals that are readily available at low costs are required. IAV DIPs typically suppress a wide range of IAV strains including contemporary human epidemic, pandemic and even highly pathogenic avian IAV as demonstrated in vitro and in mouse and ferret

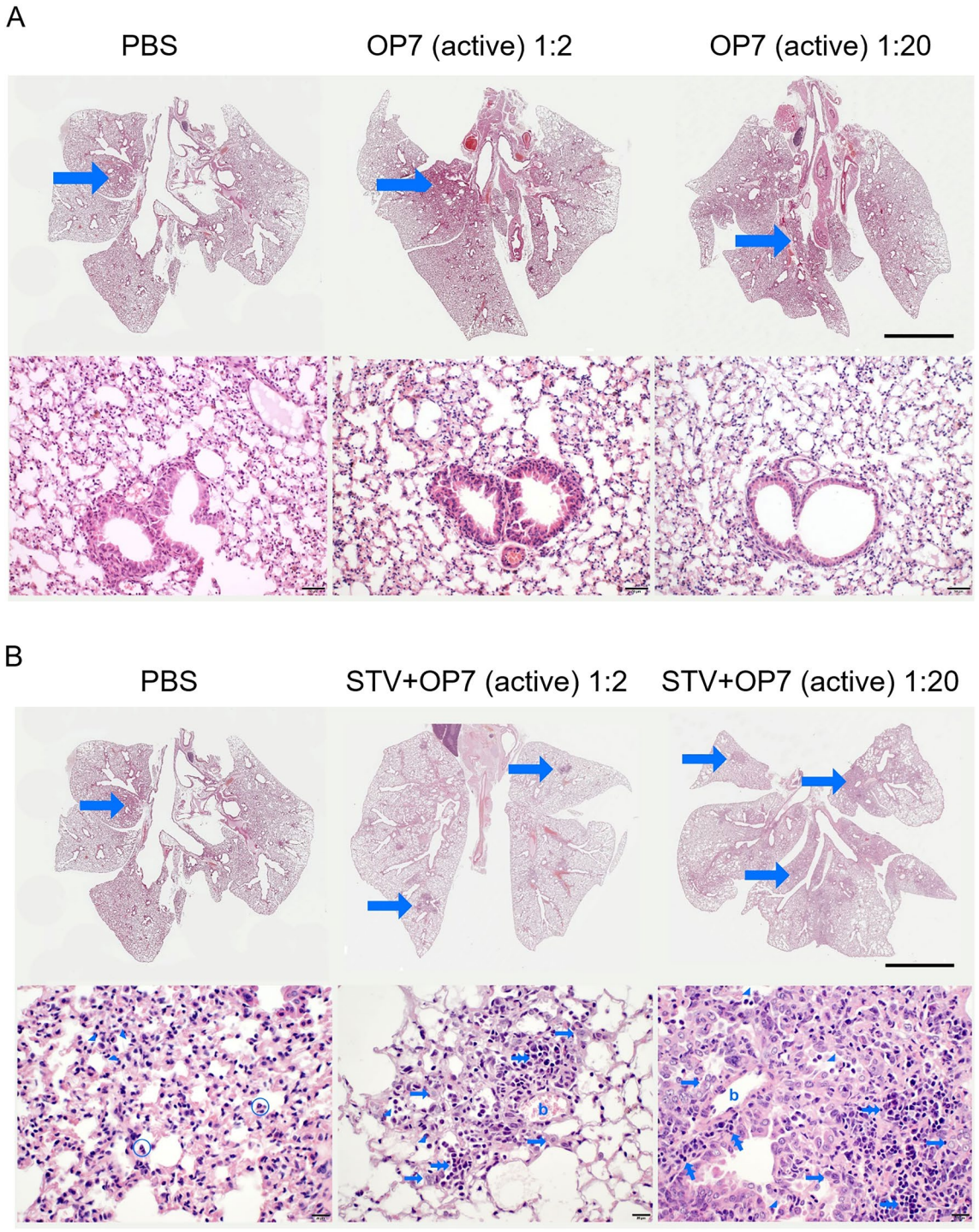


**Figure 6.** Histopathological changes in mouse lung sections after administration of OP7 chimera DIP enriched preparations and co-administration of STV with OP7 chimera DIP enriched preparations. (**A**) 20 µL of active OP7 material diluted to 1:2 ($8.96 \times 10^7$ virions/mouse) or 1:20 ($8.96 \times 10^6$ virions/mouse), or 20 µL PBS was intranasally administered to 12–24 weeks old female D2(B6).A2G-Mx1$^{r/r}$ mice (n = 5). Histopathological pictures of the lungs (14 days post infection) after hematoxylin–eosin (H&E) staining in overview (top row, bar = 1 cm) and peripheral lung in detail (bottom row, bar = 50 µm). All lungs appear almost unchanged with only minimal interstitial pneumonia located near the hilus (arrows, for detail see image in the bottom row). (**B**) Mice were co-treated by administering 20 µL volume containing a lethal dose of 1000 FFU of STV (strain PR8) with either active OP7, diluted to 1:2 ($6.5 \times 10^8$ virions/mouse) or 1:20 ($6.5 \times 10^7$ virions/mouse). Histopathological pictures of the lungs after H&E staining in overview (top row, bar = 1 cm) and areas of pneumonia in detail (bottom row, bar = 20 µm) with minimal interstitial pneumonia located near the hilus after treatment with PBS (left image), few multifocal foci of inflammation after treatment with active OP7, diluted to 1:2 (middle image) and multifocal to confluent inflammatory infiltration after treatment with active OP7, diluted to 1:20 (right image). Arrowheads: alveolar histiocytosis; encircled: neutrophils; arrows: pneumocyte type II hyperplasia; double arrows: perivascular and interstitial lymphocytic infiltration; b: blood vessel.

experiments[16,21,25,39,40]. Surprisingly, IAV DIPs can even suppress unrelated virus replication. This unspecific protection is mediated by the ability of DIPs to stimulate innate immunity and to establish a so-called antiviral state. For instance, mice were rescued from a lethal dose of influenza B virus and pneumonia virus of mice by DIP co-administration[38,41]. In addition, we demonstrated a pronounced antiviral effect against SARS-CoV-2[37] and against respiratory syncytial, yellow fever and Zika virus replication in vitro[42]. Such broad protective immunity against many different unrelated viruses was also observed for dengue and poliovirus DIPs[24,56]. This suggests that DIPs could be used as broadly-acting antiviral agents to treat viral infections as a fast countermeasure to protect people at risk and restrict virus spreading, e.g., in the case of a pandemic.

In future studies, a scalable cell culture-based production and purification process for OP7 chimera enriched DIPs should be established to achieve even higher titers and improve the purity of OP7 chimera DIP preparations. To leverage the antiviral potential of OP7 chimera DIPs, e.g. for use as an intranasal droplet spray[26,27], the establishment of a good manufacturing practice (GMP) production process would then be the base for toxicology and safety studies, clinical trials and later on to market approval.

## Materials and methods

### Cells and viruses

MDCK(adh) cells (obtained from ECACC, #84121903) and MDCK-PB2(adh) cells (expressing IAV PB2, generated by retroviral transduction, as described previously[44]) were maintained in Glasgow Minimum Essential Medium (GMEM, Thermo Fisher Scientific, #221000093) supplemented with 10% fetal bovine serum (FBS, Merck, #F7524) and 1% peptone (Thermo Fisher Scientific, #211709). Puromycin (Thermo Fisher Scientific, #A1113803) was added to a concentration of 1.5 µg/mL for MDCK-PB2(adh) cells. HEK-293T-PB2(adh) cells (expressing IAV PB2, generated previously[44]) were cultured in Dulbecco's Modified Eagle Medium (DMEM) supplemented with 10% FBS, 1% penicillin/streptomycin (10,000 units/mL penicillin and 10,000 µg/mL streptomycin, Thermo Fisher Scientific, #15140122) and puromycin at a concentration of 1 µg/mL. All adherent cells were maintained at 37 °C and 5% $CO_2$.

MDCK-PB2(sus) cells (expressing IAV PB2, previously generated by retroviral transduction[18,44]) were grown in chemically defined Xeno™ medium (Shanghai BioEngine Sci-Tech), supplemented with 8 mM glutamine and 0.5 µg/mL puromycin. Cultivation of the suspension cells was performed in shake flasks (125 mL baffled Erlenmeyer flask with vent cap, Corning, #1356244) in 50 mL working volume in an orbital shaker (Multitron Pro, Infors HT; 50 mm shaking orbit) at 185 rpm, 37 °C and 5% $CO_2$. To quantify VCC, viability and diameter of cell, Vi-cell™ XR (Beckman Coulter, #731050) was used. IAV strain PR8 (provided by Robert Koch institute, #3138) was used for the interference assay. MOIs were based on the $TCID_{50}$ titer for STV[57] (interference assay) or the plaque assay (OP7 chimera DIP material production).

### Rescue of OP7 chimera DIP

The generation of OP7 chimera DIPs was based on a previously established plasmid-based reverse genetics system for the rescue of PR8-derived Seg 1 cDIPs[44]. Here, to complement the missing PB2 protein (deleted in Seg 1 cDIPs), a co-culture of HEK-293T-PB2(adh) cells and MDCK-PB2(adh) cells were used for plasmid transfections. For rescue of OP7 chimera DIPs, a pHW-based plasmid[58] harboring the sequence of Seg 7-OP7 (GenBank accession number: MH085234) was newly generated and kindly provided by Stefan Pöhlmann and Michael Winkler (German Primate Center, Goettingen, Germany). 50 ng of this plasmid was co-transfected with 500 ng of a pHW-based plasmid harboring the deleted Seg 1 sequence of a previously described cDIP ("Seg 1 gain"[45]) and 1 µg of the remaining plasmids for Seg 2–6 and 8 (pHW192-pHW196 and pHW198[58], respectively) via the calcium phosphate-mediated transfection method. After reconstitution, OP7 chimera DIP material was amplified in MDCK-PB2(adh) cells and later used to infect MDCK-PB2(sus) cells for seed virus production.

### OP7 chimera DIP material production in shake flasks

Production of OP7 chimera DIP preparations in shake flasks using MDCK-PB2(sus) cells was conducted with complete medium exchange prior to infection as described previously[18,43]. In brief, cells in exponential growth phase were centrifuged (300×*g*, 5 min, room temperature) and resuspended in fresh medium (without puromycin) containing trypsin (final activity 20 U/mL, Thermo Fisher Scientific, #27250-018) at $2.0 \times 10^6$ cells/mL. Cells were infected at different MOIs ranging from 1E-2 to 1E-5 at 37 °C and 5% $CO_2$. At indicated time points, samples were centrifuged (3000×*g*, 4 °C, 10 min) and supernatants were stored at -80 °C until further analysis. RNA of progeny virions was extracted from supernatants using the NucleoSpin RNA virus kit (Macherey–Nagel, #740956) according to the manufacturer's instructions and stored at -80 °C until PCR-based analysis.

OP7 chimera DIP material for mouse infection studies was produced in shake flasks at a MOI of 1E-4. Harvested DIP material was clarified (3000×*g*, 10 min and 4 °C) and sucrose (Merck, #84097) was added at a final concentration of 4%. Next, the material was purified and concentrated by SXC as previously described[18,19,48]. Part of the purified, concentrated and sterile filtered DIP material was UV inactivated for 24 min. Active (no UV inactivation), inactive (UV inactivated) DIP material and PBS spiked with sucrose (4% final concentration) were stored at − 80 °C until further use.

### Virus quantification

Infectious virus titers were quantified using the plaque assay as previously described[18,19,39] using MDCK(adh) cells (interfering assay) or MDCK-PB2(adh) cells (determination of OP7 chimera DIP containing seed virus titer). Infectious virus titers were expressed as plaque-forming units (PFU)/mL. Furthermore, total virus concentrations were quantified using the HA assay as previously described[59].

## Segment-specific RT-PCR

To detect contaminating DI vRNAs in Seg 2-Seg 8 in progeny virions, purified extracellular RNA was subjected to segment-specific PCR as described previously[39,54]. In brief, RNA was reverse transcribed to cDNA using a universal "Uni12" primer[60] that binds to all eight genome segments. The resulting cDNA samples were used to amplify each genomic segment individually using segment-specific primers. PCR products were analyzed by agarose gel electrophoresis.

## RT-qPCR

In order to quantify the vRNAs purified from progeny virions, we used a previously described RT-qPCR method that enables polarity- and gene-specific quantification of individual vRNAs[19,39,54]. For this, a methodology involving tagged primers was employed[61]. Primers used for quantification of the vRNA of Seg 5 are listed in[39,54], for Seg 7-OP7 in[19], and for Seg 7-WT, new primers were designed for the present study (for reverse transcription, Seg 7-WT tagRT for: 5′-ATTTAGGTGACACTATAGAAGCGTCTCGCTATTGCCGCAAA-3′ and for qPCR, Seg 7-WT realtime rev: 5′-CCTTTCAGTCCGTATTTAAAGC-3′). In order to allow for absolute quantification, RNA reference standards were used. vRNA concentrations were calculated based on calibration curves.

## Interference assay

The produced OP7 chimera DIP material was tested for the interfering efficacy in vitro according to a previously established protocol[19,39]. Here, we assessed the inhibition of STV propagation upon co-infection with OP7 chimera DIP preparations. After infection, supernatants were analyzed for infectious and total virus titers using the plaque and HA assay, respectively. RT-qPCR and MS were used for quantification of vRNA and viral protein, respectively, of the progeny virions.

## Quantification of IAV proteins

MS analysis was used for absolute quantification of M1-WT, M1-OP7 and NP according to a method described previously[46]. For this, we used isotopically labelled peptides of synthetic origin of corresponding proteins that were added as an internal standard before tryptic digestion of the samples for absolute quantification (AQUA). For M1-OP7, a peptide containing one mutation, which is not present in the M1-WT (EITFYGAK) was used. For quantification of M1-WT, two peptides exclusive for M1-WT (LEDVFAGK, QMVTTTNPLIR) were used. In brief, supernatant samples containing DIPs were heat inactivated (3 min, 80 °C) for further processing. Next, total protein concentration was determined using a Pierce® BCA protein assay (Thermo Fisher Scientific, #23227) according to the manufacturer's protocol. Sample preparation for MS analysis was performed by using filter-aided sample preparation as described previously[46,62]. After drying of the eluted peptides, 80 µL of mobile phase A (LC–MS-grade water, 0.1% trifluoroacetic acid) and 20 µL (= 2 pmol of each peptide) of peptide standard mix containing isotopically labelled peptides of synthetic origin for M1-WT, M1-OP7 and NP were added to each sample. Subsequently, MS analysis was carried out as described before[46]. Raw files from Bruker timsTOF Pro were analysed by using Skyline (vs. 19.1)[63]. Absolute protein copy numbers and virus concentrations were calculated as described previously[46].

## Mouse infection experiments

D2(B6).A2G-Mx1$^{r/r}$ mice were generated by backcrossing DBA/2JRj mice for 10 generations onto congenic B6.A2G-Mx1r/r mice as described previously[53]. Mice were bred and maintained in individually ventilated cages in a specific pathogen-free environment as per relevant guidelines and regulations (animal facility, Helmholtz Centre for Infection Research, Braunschweig Germany); food and water were provided ad libitum. Female, age-matched (12–24 weeks) D2(B6).A2G-Mx1$^{r/r}$ mice that harbor a functional MX dynamin-like GTPase 1 (Mx1) resistance gene were randomly allocated into experimental groups. Following intraperitoneal injection of ketamine/xylazine, mice were intranasally administered with 20 µL of active OP7 chimera DIPs or PBS at indicated concentrations to test for the tolerability. Moreover, antiviral efficacy was studied by inoculation with a lethal dose of 1000 FFU of IAV STV strain PR8 and co-treatment with active OP7 chimera DIP enriched preparations at indicated concentrations, inactive OP7 chimera DIP enriched preparations or PBS in a total volume of 20 µL. Determination of the FFU titer was conducted as described elsewhere[64]. Following administration, health status (body weight, appearance of fur, posture, activity) of mice was monitored at least once per day. In case humane endpoint criteria were reached, animals were humanely euthanized (via isoflurane inhalation and subsequent exsanguination) and the infection was recorded as lethal (AVMA guidelines were adhered). BAL samples were harvested as described previously[65]. Serum albumin concentrations in BAL fluids were measured by ELISA (Fortis Life Sciences, #E90-134).

## Histopathological analysis

Complete lungs of the mice were routinely fixed in 4% formalin and embedded in paraffin. Sections with 5 µm thickness were cut, dewaxed, and stained with hematoxylin–eosin (H&E). Histopathological evaluation was performed in a blinded manner by a veterinary pathologist certified by the European College of Veterinary Pathologists.

## Statistical analysis

All the statistical analysis and graph generation were performed using GraphPad Prism 9 software.

## Approval for animal experiments

Animals were maintained and treated as per ARRIVE guidelines. All in vivo experiments were conducted after review and approval of the study protocol by institutional (Helmholtz Centre for Infection Research) and regional ethical bodies (Niedersaechsisches Landesamt fuer Verbraucherschutz und Lebensmittelsicherheit, LAVES 33.19-42502-04-18/2922).

## Data availability

Data generated during this study can be requested from the corresponding co-author upon request.

Received: 21 August 2023; Accepted: 15 November 2023
Published online: 28 November 2023

## References

1. Qiu, Z. & Feng, Z. Transmission dynamics of an influenza model with vaccination and antiviral treatment. *Bull. Math. Biol.* **72**, 1–33 (2010).
2. Taubenberger, J. K., Reid, A. H. & Fanning, T. G. The 1918 influenza virus: A killer comes into view. *Virology* **274**(2), 241–245 (2000).
3. Chen, J. *et al.* Advances in development and application of influenza vaccines. *Front. Immunol.* **12**, 711997 (2021).
4. Alnaji, F. G. & Brooke, C. B. Influenza virus DI particles: Defective interfering or delightfully interesting?. *PLoS Pathog.* **16**(5), e1008436 (2020).
5. Chaturvedi, S. *et al.* Identification of a therapeutic interfering particle-A single-dose SARS-CoV-2 antiviral intervention with a high barrier to resistance. *Cell* **184**(25), 6022–6036 (2021).
6. Girgis, S. *et al.* Evolution of naturally arising SARS-CoV-2 defective interfering particles. *Commun. Biol.* **5**(1), 1140 (2022).
7. Kalamvoki, M. & Norris, V. A defective viral particle approach to COVID-19. *Cells* **11**(2), 1 (2022).
8. Levi, L. I. *et al.* Defective viral genomes from chikungunya virus are broad-spectrum antivirals and prevent virus dissemination in mosquitoes. *PLoS Pathog.* **17**(2), e1009110 (2021).
9. Li, D. *et al.* Dengue virus-free defective interfering particles have potent and broad anti-dengue virus activity. *Commun. Biol.* **4**(1), 557 (2021).
10. Mendes, M. & Russell, A. B. Library-based analysis reveals segment and length dependent characteristics of defective influenza genomes. *PLoS Pathog.* **17**(12), e1010125 (2021).
11. Rezelj, V. V. *et al.* Defective viral genomes as therapeutic interfering particles against flavivirus infection in mammalian and mosquito hosts. *Nat. Commun.* **12**(1), 2290 (2021).
12. Rudiger, D. *et al.* Multiscale modeling of influenza A virus replication in cell cultures predicts infection dynamics for highly different infection conditions. *PLoS Comput. Biol.* **15**(2), e1006819 (2019).
13. Smither, S. J. *et al.* An investigation of the effect of transfected defective, ebola virus genomes on ebola replication. *Front. Cell Infect. Microbiol.* **10**, 159 (2020).
14. Tilston-Lunel, N. L. *et al.* Sustained replication of synthetic canine distemper virus defective genomes in vitro and in vivo. *mSphere* **6**(5), e0053721 (2021).
15. Wang, S. *et al.* Subgenomic RNA from dengue virus type 2 suppresses replication of dengue virus genomes and interacts with virus-encoded NS3 and NS5 proteins. *ACS Infect. Dis.* **6**(3), 436–446 (2020).
16. Zhao, H. *et al.* Dual-functional peptide with defective interfering genes effectively protects mice against avian and seasonal influenza. *Nat. Commun.* **9**(1), 2358 (2018).
17. Yao, S. *et al.* A synthetic defective interfering SARS-CoV-2. *PeerJ* **9**, e11686 (2021).
18. Hein, M. D. *et al.* Cell culture-based production and in vivo characterization of purely clonal defective interfering influenza virus particles. *BMC Biol.* **19**(1), 91 (2021).
19. Hein, M. D. *et al.* OP7, a novel influenza A virus defective interfering particle: Production, purification, and animal experiments demonstrating antiviral potential. *Appl. Microbiol. Biotechnol.* **105**(1), 129–146 (2021).
20. Zhao, H. *et al.* Peptidic defective interfering gene nanoparticles against Omicron, Delta SARS-CoV-2 variants and influenza A virus in vivo. *Signal Transduct. Target Ther.* **7**(1), 266 (2022).
21. Huo, C. *et al.* Defective viral particles produced in mast cells can effectively fight against lethal influenza A virus. *Front. Microbiol.* **11**, 553274 (2020).
22. Huo, C. *et al.* Safety, immunogenicity, and effectiveness of defective viral particles arising in mast cells against influenza in mice. *Front. Immunol.* **11**, 585254 (2020).
23. Welch, S. R. *et al.* Defective interfering viral particle treatment reduces clinical signs and protects hamsters from lethal nipah virus disease. *mBio.* **13**(2), e0329421 (2022).
24. Xiao, Y. *et al.* A defective viral genome strategy elicits broad protective immunity against respiratory viruses. *Cell* **184**(25), 6037–6051 (2021).
25. Dimmock, N. J. *et al.* Influenza virus protecting RNA: An effective prophylactic and therapeutic antiviral. *J. Virol.* **82**(17), 8570–8578 (2008).
26. Dimmock, N. J. & Easton, A. J. Cloned defective interfering influenza RNA and a possible pan-specific treatment of respiratory virus diseases. *Viruses* **7**(7), 3768–3788 (2015).
27. Dimmock, N. J. & Easton, A. J. Defective interfering influenza virus RNAs: Time to reevaluate their clinical potential as broad-spectrum antivirals?. *J. Virol.* **88**(10), 5217–5227 (2014).
28. Bdeir, N. *et al.* Evidence that two instead of one defective interfering RNA in influenza A virus-derived defective interfering particles (DIPs) does not enhance antiviral activity. *Sci. Rep.* **11**(1), 20477 (2021).
29. Wang, C. *et al.* Cell-to-cell variation in defective virus expression and effects on host responses during influenza virus infection. *J. Biol* **11**(1), 1 (2020).
30. Alnaji, F. G. *et al.* Influenza A virus defective viral genomes are inefficiently packaged into virions relative to wild-type genomic RNAs. *mBio* **12**(6), e0295921 (2021).
31. Boergeling, Y. *et al.* Evidence for a novel mechanism of influenza virus-induced type I interferon expression by a defective rna-encoded protein. *PLoS Pathog.* **11**(5), e1004924 (2015).
32. Nayak, D. P., Chambers, T. M. & Akkina, R. K. Defective-interfering (DI) RNAs of influenza viruses: origin, structure, expression, and interference. *Curr. Top. Microbiol. Immunol.* **114**, 103–151 (1985).
33. Laske, T. *et al.* Modeling the intracellular replication of influenza A virus in the presence of defective interfering RNAs. *Virus Res.* **213**, 90–99 (2016).
34. Duhaut, S. D. & McCauley, J. W. Defective RNAs inhibit the assembly of influenza virus genome segments in a segment-specific manner. *Virology* **216**(2), 326–337 (1996).

35. Ziegler, C. M. & Botten, J. W. Defective interfering particles of negative-strand RNA viruses. *Trends Microbiol.* **28**(7), 554–565 (2020).
36. Yang, Y. C. *et al.* The antiviral and antitumor effects of defective interfering particles/genomes and their mechanisms. *Front. Microbiol.* **10**, 1 (2019).
37. Rand, U. *et al.* Antiviral activity of influenza a virus defective interfering particles against SARS-CoV-2 replication in vitro through stimulation of innate immunity. *Cells* **10**(7), 1 (2021).
38. Scott, P. D. *et al.* Defective interfering influenza A virus protects in vivo against disease caused by a heterologous influenza B virus. *J. Gen. Virol.* **92**(Pt 9), 2122–2132 (2011).
39. Kupke, S. Y. *et al.* A novel type of influenza a virus-derived defective interfering particle with nucleotide substitutions in its genome. *J. Virol.* **93**(4), 1 (2019).
40. Dimmock, N. J. *et al.* Cloned defective interfering influenza virus protects ferrets from pandemic 2009 influenza A virus and allows protective immunity to be established. *PLoS One* **7**(12), e49394 (2012).
41. Easton, A. J. *et al.* A novel broad-spectrum treatment for respiratory virus infections: Influenza-based defective interfering virus provides protection against pneumovirus infection in vivo. *Vaccine* **29**(15), 2777–2784 (2011).
42. Pelz, L. *et al.* Broad-spectrum antiviral activity of Influenza A defective interfering particles against respiratory syncytial, Yellow Fever, and Zika Virus replication in vitro. *Viruses* **15**(9), 1 (2023).
43. Hein, M. D. *et al.* Cell culture-based production of defective interfering influenza A virus particles in perfusion mode using an alternating tangential flow filtration system. *Appl. Microbiol. Biotechnol.* **105**(19), 7251–7264 (2021).
44. Bdeir, N. *et al.* A system for production of defective interfering particles in the absence of infectious influenza A virus. *PLoS One* **14**(3), e0212757 (2019).
45. Pelz, L. *et al.* Semi-continuous propagation of Influenza A virus and its defective interfering particles: Analyzing the dynamic competition to select candidates for antiviral therapy. *J. Virol.* **95**(24), e0117421 (2021).
46. Küchler, J. *et al.* Absolute quantification of viral proteins during single-round replication of MDCK suspension cells. *J. Proteom.* **259**, 104544 (2022).
47. Genzel, Y. *et al.* MDCK and Vero cells for influenza virus vaccine production: A one-to-one comparison up to lab-scale bioreactor cultivation. *Appl. Microbiol. Biotechnol.* **88**(2), 461–475 (2010).
48. Marichal-Gallardo, P. *et al.* Steric exclusion chromatography for purification of cell culture-derived influenza A virus using regenerated cellulose membranes and polyethylene glycol. *J. Chromatogr. A* **1483**, 110–119 (2017).
49. Marichal-Gallardo, P. *et al.* Single-use capture purification of adeno-associated viral gene transfer vectors by membrane-based steric exclusion chromatography. *Hum. Gene Ther.* **32**(17–18), 959–974 (2021).
50. Wiley, J. A. *et al.* Inducible bronchus-associated lymphoid tissue elicited by a protein cage nanoparticle enhances protection in mice against diverse respiratory viruses. *PLoS One* **4**(9), e7142 (2009).
51. Kim, C. U. *et al.* Influenza viral matrix 1 protein aggravates viral pathogenicity by inducing TLR4-mediated reactive oxygen species production and apoptotic cell death. *Cell Death Dis.* **14**(3), 228 (2023).
52. Schmit, T. *et al.* Interferon-gamma promotes monocyte-mediated lung injury during influenza infection. *Cell Rep.* **38**(9), 110456 (2022).
53. Shin, D. L. *et al.* Protection from severe influenza virus infections in mice carrying the Mx1 influenza virus resistance gene strongly depends on genetic background. *J. Virol.* **89**(19), 9998–10009 (2015).
54. Frensing, T. *et al.* Impact of defective interfering particles on virus replication and antiviral host response in cell culture-based influenza vaccine production. *Appl. Microbiol. Biotechnol.* **98**(21), 8999–9008 (2014).
55. Rudiger, D. *et al.* Multiscale model of defective interfering particle replication for influenza A virus infection in animal cell culture. *PLoS Comput. Biol.* **17**(9), e1009357 (2021).
56. Lin, M. H. *et al.* Defective interfering particles with broad-acting antiviral activity for dengue, Zika, Yellow Fever, respiratory syncytial and SARS-CoV-2 virus infection. *Microbiol. Spectr.* **10**(6), e0394922 (2022).
57. Genzel, Y. & Reichl, U. Vaccine production. In *Animal Cell Biotechnology* (ed. Portner, R.) 457–473 (Humana Press, 2007).
58. Hoffmann, E. *et al.* A DNA transfection system for generation of influenza A virus from eight plasmids. *Proc. Natl. Acad. Sci. USA* **97**(11), 6108–6113 (2000).
59. Kalbfuss, B. *et al.* Monitoring influenza virus content in vaccine production: Precise assays for the quantitation of hemagglutination and neuraminidase activity. *Biologicals* **36**(3), 145–161 (2008).
60. Hoffmann, E. *et al.* Universal primer set for the full-length amplification of all influenza A viruses. *Arch. Virol.* **146**(12), 2275–2289 (2001).
61. Kawakami, E. *et al.* Strand-specific real-time RT-PCR for distinguishing influenza vRNA, cRNA, and mRNA. *J. Virol. Methods* **173**(1), 1–6 (2011).
62. Wiśniewski, J. R. *et al.* Universal sample preparation method for proteome analysis. *Nat. Methods* **6**(5), 359–362 (2009).
63. MacLean, B. *et al.* Skyline: An open source document editor for creating and analyzing targeted proteomics experiments. *Bioinformatics* **26**(7), 966–968 (2010).
64. Lambertz, R. L. O. *et al.* Exchange of amino acids in the H1-haemagglutinin to H3 residues is required for efficient influenza A virus replication and pathology in Tmprss2 knock-out mice. *J. Gen. Virol.* **99**(9), 1187–1198 (2018).
65. Sharma-Chawla, N. *et al.* In vivo neutralization of pro-inflammatory cytokines during secondary streptococcus pneumoniae infection post Influenza A virus infection. *Front. Immunol.* **10**, 1864 (2019).


## Acknowledgements

For the excellent technical assistance we thank Claudia Best, Nancy Wynserski, and Karin Lammert. Xeno™ medium used in the study was kindly supplied by Shanghai BioEngine Sci-Tech and Prof. Tan from the East China University of Science and Technology. We would like to thank Prof. Stefan Pöhlmann and Michael Winkler from the German Primate Center, Goettingen, Germany for providing WT IAV segments and Seg 7-OP7 vRNA encoding plasmids.

## Author contributions

Conceptualization, T.D., L.P., M.D.H., S.Y.K., and U.R.; formal analysis, L.P., J.B.; funding acquisition, A.G, D.B. (Dunja Bruder), U.R.; investigation, T.D., L.P., J.B., J.K., O.K., P.M., M.B.; project administration, T.D., L.P., S.Y.K.; supervision, D.B. (Dirk Benndorf), A.G., Y.G., D.B. (Dunja Bruder), S.Y.K., U.R.; visualization, T.D., L.P., O.K., S.Y.K.; writing—original draft, T.D.; L.P.; writing—review and editing, T.D., L.P., J.B., J.K., O.K., P.M., M.B., M.D.H, A.G., D.B. (Dirk Benndorf), Y.G., D.B. (Dunja Bruder), S.Y.K., U.R..

## Funding

Open Access funding enabled and organized by Projekt DEAL.

## Competing interests

A patent to treat IAV infections with OP7 as an antiviral agent is pending. Patent holders are S.Y.K. and U.R. Another patent about treating coronavirus infection using DI244 and OP7 as antiviral agents is pending. Patent holders are S.Y.K., U.R., M.D.H., D.B. (Dunja Bruder). All other authors declare that they do not hold any competing interest.

## Additional information

**Supplementary Information** The online version contains supplementary material available at https://doi.org/10.1038/s41598-023-47547-1.

**Correspondence** and requests for materials should be addressed to S.Y.K.

**Reprints and permissions information** is available at www.nature.com/reprints.

**Publisher's note** Springer Nature remains neutral with regard to jurisdictional claims in published maps and institutional affiliations.